Acoustooptic Resonance in Deep-Etched GaAs–AlGaAs Electrooptic Modulators

Christopher D. Watson, Maxime Poirier, John M. Heaton, *Member, IEEE, Member, OSA*, Meirion Lewis, and Marcel Boudreau

Abstract—Deep-etched GaAs–AlGaAs waveguide modulators are shown to generate acoustic waves that can cause elastooptic anomalies in the modulator response. The theory of acoustooptic interactions in linear electrooptic modulators is described and a one-dimensional (1-D) approximation of a deep-etched GaAs–AlGaAs waveguide modulator is developed. The 1-D theory is shown to predict the acoustooptic resonance phenomena that is seen in experimental devices.

Index Terms—Acoustooptic, elastooptic, electrooptic modulator (EOM), gallium arsenide, ridge waveguide.

I. INTRODUCTION

IN semiconductor electrooptic modulators (EOMs), high-modulation efficiency can be achieved by applying the modulating voltage to a reverse-bias diode whose depletion region forms the waveguide core. This arrangement can be accomplished on GaAs by etching a ridge into a p-i-n doped slab waveguide that is composed of epitaxial GaAs–AlGaAs layers [1]. Usually, in order to minimize waveguide loss, this ridge is shallow-etched such that only the upper cladding of the planar waveguide is penetrated. Using this approach, low voltage, low-loss modulators optimized for both 10- and 40-Gb/s applications have been demonstrated [2] and have been commercially available for some time. In more complex optical circuits [3], [4], however, the weak horizontal optical confinement of the shallow-etched waveguide can be problematic. In particular, the implementation of waveguide bends and the avoidance of optical crosstalk require both careful design and accurate fabrication.

To alleviate these difficulties, deep-etched waveguides have been proposed for integrated optic devices on GaAs [5], [6]. In this type of waveguide, the etch depth extends through the waveguide core into a lower cladding region that is carefully designed to leak higher order modes. This results in a waveguide with strong horizontal confinement that is better suited to the fabrication of tight bends and closely spaced waveguides. In modulator design, deep-etched waveguides would also seem to offer the additional benefits of reduced capacitance and optimum electrooptic overlap. However, the use of deep-etched waveguides in modulator applications should be approached with some caution as this geometry is susceptible to acoustooptic-generated resonance in the modulator response: when an electric field is applied to an unconstrained linear electrooptic crystal, a mechanical deformation of the material occurs as a result of the converse piezoelectric effect [7]. In deep-etched modulators, this material strain appears as acoustic waves that are generated by the exposed depletion field and then confined by the vertical sidewalls. At critical frequencies, transverse acoustic resonance of the ridge occurs and results in a mechanical distortion of the waveguide core. Consequently, at the resonant frequencies, the electrooptic effect is accompanied by a strong elastooptic effect that can dominate the modulator response. Typically, these elastooptic anomalies occur in the gigahertz regime and can cause patterning in 10-Gb/s applications. Unfortunately, in deep-etched GaAs–AlGaAs waveguides, these anomalies are difficult to suppress without compromising other device characteristics, and so this type of waveguide must be used with care in broad-band modulator applications.

Section II of this paper describes the theory of acoustooptic interactions in linear EOMs and develop a one-dimensional (1-D) analysis that is appropriate to deep-etched GaAs–AlGaAs devices. In Section III, this 1-D model is compared with the experiment and good agreement is found.

II. THEORY

Fig. 1 shows a schematic diagram of a GaAs–AlGaAs electrooptic phase modulator that is based on a deep-etched waveguide. The waveguide has a width g and is formed by etching vertical sidewalls into a planar waveguide. Strong lateral optical confinement is achieved by ensuring that the etch depth h extends through the waveguide core into the lower cladding layer. In this configuration, the modulating voltage is applied between the substrate and a Shottky contact so that a depletion field forms in the undoped core and upper cladding regions of the waveguide. The electric field of the depletion region, which is substantially parallel to the waveguide sidewalls, terminates on a depletion stop that is aligned with the bottom of the waveguide core.

The piezoelectric-induced distortion of the waveguide cross section is described by the material strain $\boldsymbol{S}$, which is expressed in terms of a particle displacement

$$S_{ij} = \frac{\left(\frac{\partial u_i}{\partial x_j} + \frac{\partial u_j}{\partial x_i} \right)}{2} \tag{1}$$

where u_i is the set of particle displacement $\{u, v, w\}$; x_i are the axes $\{x, y, z\}$ as shown in Fig. 1; and summation is implied over repeated indexes. The coupling between the electrical and mechanical fields caused by the piezoelectric effect is described
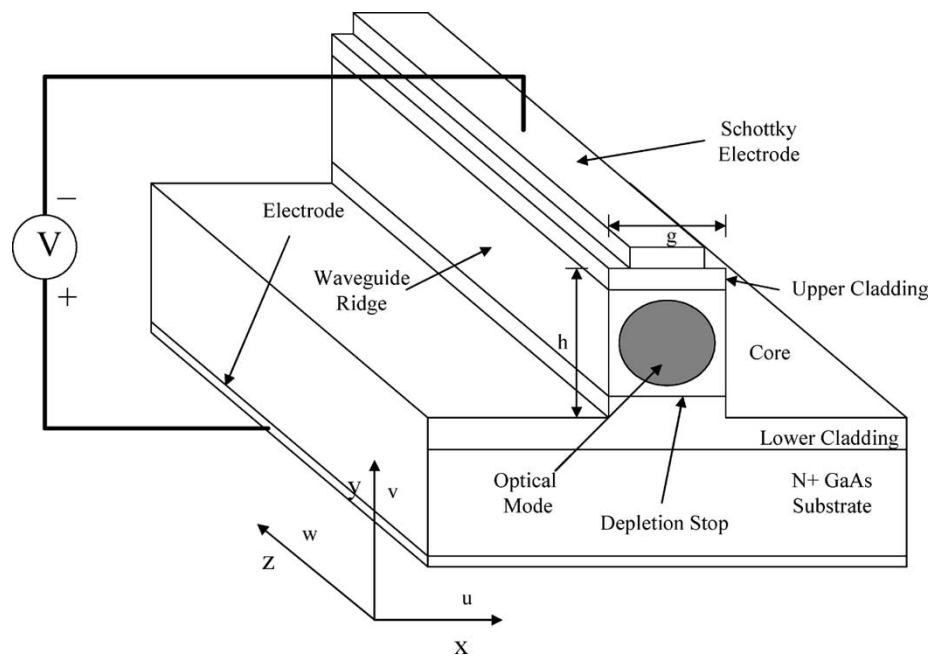
Fig. 1.   Schematic diagram of a deep-etched GaAs–AlGaAs EOM.

by the material constitutive relations for stress $\boldsymbol{T}$ and electric displacement $\boldsymbol{D}$

$$T_{ij} = c_{ijkl}S_{kl} - e_{lij}E_l \tag{2a}$$
$$D_j = e_{jkl}S_{kl} + \varepsilon_{jl}E_l \tag{2b}$$

where $\boldsymbol{e}$ is the third-rank piezoelectric tensor, $\boldsymbol{c}$ is the fourth-rank stiffness tensor at zero electric field, ε is permittivity tensor at zero strain, and $\boldsymbol{E}$ is the electric field. Under modulation, the waveguide core is set in motion because of (2), and this motion must satisfy Newton's second law [7]

$$\frac{\partial T_{ij}}{\partial x_j} = \rho \frac{\partial^2 u_i}{\partial t^2} \tag{3}$$

where ρ is the material density. In addition, the electromagnetic fields must also satisfy Maxwell's equations, which under the quasistatic approximation, and neglecting charge in the depletion region reduce to [8]

$$\frac{\partial D_i}{\partial x_i} = 0. \tag{4}$$

The effect of the material strain is to modify the optical index of the crystal through the elastooptic effect. Consequently, the electric field in the waveguide causes both an electrooptic and elastooptic effect. The composite response is described in terms of the change in the dielectric impermeability tensor $\boldsymbol{B}$

$$\Delta B_{ij} = r_{ijk}E_k + p_{ijrs}S_{rs} \tag{5}$$

where r_{ijk} is the third-rank linear electrooptic tensor measured under conditions of zero strain, and p_{ijrs} is the fourth-rank elastooptic tensor [7].

Equations (1)–(5) provide the basic framework to analyze acoustooptic interactions in linear EOMs. For the device in Fig. 1, the dimension of the structure in the z direction is large in comparison with the other two directions (x and y). In this
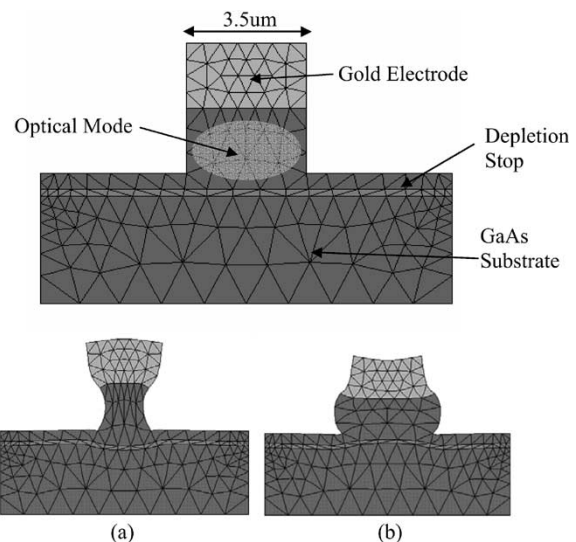

Fig. 2.   Distortion of a 3.5-μm-wide ridge caused by an applied voltage in a deep-etched GaAs–AlGaAs modulator ($\times 10^6$). (a) 1 V between electrode and depletion stop. (b) -1 V between electrode and depletion stop.

case, (1)–(5) can be simplified by using the plane strain approximation which assumes $w = 0$ and $\partial/\partial z = 0$. Once (1)–(5) have been expanded under the plane strain approximation, the solution can be determined numerically. Typical numerical results showing the piezoelectric-induced distortion caused by the depletion field in a deep-etched waveguide are displayed in Fig. 2. These results, which were computed using commercially available software [9], are included for illustration only.

Although a numerical solution has the benefit of accounting for all types of elastic wave propagation, greater physical insight is achieved by solving the equations analytically in one dimension. The structure in Fig. 1 can be reduced to one dimension by noting that the piezoelectric and electrooptic tensors have

the same symmetry; and as a consequence, an electric field E_y will cause both a change in the optical index seen by a transverse-electric (TE) wave (optical electric field polarized along x) and also a stress along the x axis. This stress, depending upon the mechanical constraints, will cause a strain along the x axis, which will then modulate the TE index through the elastooptic effect. Therefore, a 1-D analysis in which both the strain and variation along the y and z axis are neglected is appropriate. This approximation corresponds to the situation in which $h \gg g$ which is not the case for typical deep-etched devices. Nevertheless, as is shown in Section III, a 1-D model based upon this approximation is quite successful in predicting the behavior of real devices.

A. 1-D Analysis

The 1-D approximation of a deep-etched modulator is shown in Fig. 3. The structure comprises three layers: two semi-infinite damping regions, which are isotropic and nonpiezoelectric, and a GaAs core. The GaAs core represents the GaAs–AlGaAs epitaxial stack shown in Fig. 1, and this approximation is justified by the similar material properties of these compounds. The damping layers, which are not present in Fig. 1, are included to account for the loss of acoustic energy that would occur in a real structure through the excitation of bulk and surface acoustic waves.

When a uniform electric field E_y is applied along the [100] crystal axis, the constitutive relations for the material become

$$T_{xx}(x) = c'_{11}S_{xx}(x) + e_{14}E_y \qquad (6a)$$

$$D_y(x) = \varepsilon E_y - e_{14}S_{xx}(x) \qquad (6b)$$

where $T_{xx}(x)$ is the stress normal to the material interface, c'_{11} is the appropriate element of the c' written in contracted notation; and c' is determined by rotating c to account for the [011] direction of the waveguides shown in Fig. 3. Substitution of (6) into (3) with an assumed time dependence of $e^{j\omega t}$ yields the acoustic-wave equation in terms of particle displacement

$$\frac{d^2u(x)}{dx^2} + k^2u(x) = -\frac{d(e_{14}E_y)}{dx} \qquad (7)$$

where $k = \omega/v_p$ is the wavenumber and $v_p = \sqrt{c'_{11}/\rho}$ is the velocity of an x-propagating ($[0\bar{1}1]$-directed) longitudinal elastic wave and $c'_{11} = (c_{11} + c_{12} + 2c_{44})/2$. The term on the right-hand side (RHS) of (7) is zero everywhere except at the boundary but is included to emphasize that the source of the acoustic waves is the depletion region at the waveguide sidewall. Equation (7) is readily solved to give

$$u(x) = \begin{cases} \psi_1 \exp(\pm jk_1 x), & |x| > a \\ \psi_2 \sin(k_2 x), & -a \leq x \leq a \end{cases} \qquad (8)$$

where $\psi_{1,2}$ are the wave amplitudes and the subscript "1" refers to the damping region and the subscript "2" refers to the core region. $\psi_{1,2}$ are determined by applying continuity of $u(x)$ and $T_{xx}(x)$ at the boundaries

$$\begin{pmatrix} \psi_1 \\ \psi_2 \end{pmatrix} = \begin{pmatrix} -\exp(-jk_1 a), & \sin(k_2 a) \\ jk_1 \, c'_{11}|_1 \exp(-jk_1 a), & k_2 \, c'_{11}|_2 \cos(k_2 a) \end{pmatrix}^{-1}$$
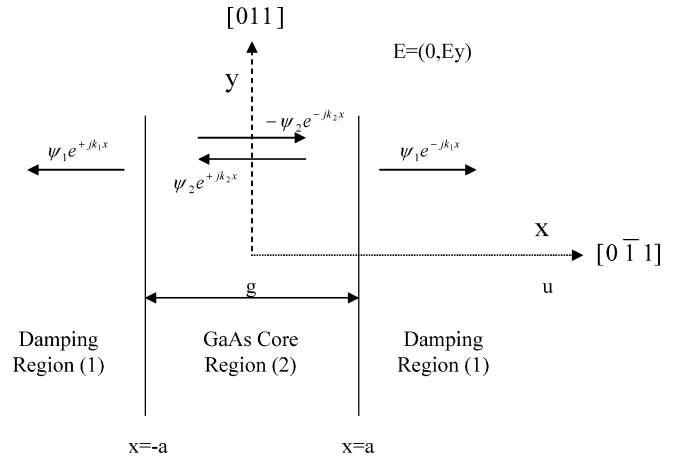$$\times \begin{pmatrix} 0 \\ -e_{41}E_y \end{pmatrix}. \qquad (9)$$

Fig. 3. One-dimensional representation of a deep-etched GaAs–AlGaAs modulator.

Solving (9) yields the strain in the core region as

$$S_{xx}^c(x) = \frac{-e_{14}E_y k_2 \cos(k_2 x)}{\omega Z_2 \cos(k_2 a) + j\omega Z_1 \sin(k_2 a)} \qquad (10)$$

where $Z = \rho v_p$ is the acoustic impedance.

The effect of E_y and $S_{xx}^c(x)$ on the index of the waveguide core is described by (5), and in the case of TE-polarized light, the composite response leads to an index change given by

$$\Delta n^{TE} = \frac{1}{2}n_0^3 \left(r_{41}E_y - \frac{(p_{11} + p_{12} + 2p_{44})}{2}S_{xx}^c(x) \right) \quad (11)$$

where n_0 is the refractive index of GaAs. In addition, because of the symmetry of p, $S_{xx}^c(x)$ affects all the diagonal components of the dielectric impermeability tensor. Consequently, the elastooptic effect, unlike the electrooptic effect, causes both a TE and a transverse-magnetic (TM) response. The index change for TM-polarized light is determined from (5) as

$$\Delta n^{TM} = -\frac{1}{2}n_0^3 p_{12}S_{xx}^c(x). \qquad (12)$$

Ultimately, the modulator response M is determined by calculating the overlap of the optical intensity with the index change. For deep-etched waveguides, the optical field for both TE and TM is cosinusoidal within the waveguide core and so M is given by

$$M^{TE,TM} \propto \int_{-a}^{a} \Delta n^{TE,TM} \cos^2\left(\frac{\pi x}{2a}\right) dx. \qquad (13)$$

In the following section, the 1-D model described by (13) is compared with the experiment.

III. COMPARISON WITH EXPERIMENT

Fig. 4 shows the wide-band optical response of a deep-etched GaAs–AlGaAs electrooptic Mach–Zehnder intensity modulator. The intensity modulator was formed from two identical phase modulators that were connected in a series push–pull configuration. The measurements were made using an HP8703a (a lightwave component analyzer) with > 20 dB polarizers set to pass TE-polarized light on both the input and output optical ports. The inset to Fig. 4 is an scanning electron microscope (SEM) of a typical modulator ridge and shows a ridge width
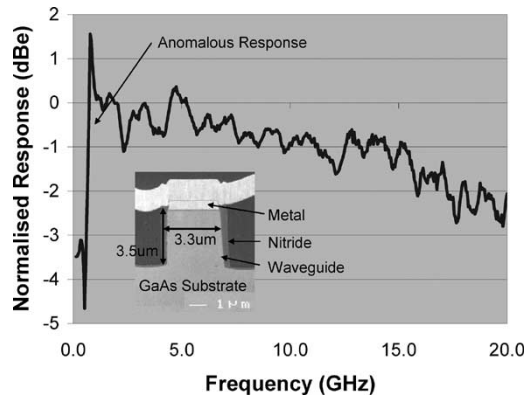
Fig. 4. Measured TE response of a deep-etched GaAs–AlGaAs electrooptic intensity modulator. Inset shows an SEM of the modulator waveguide ridge.
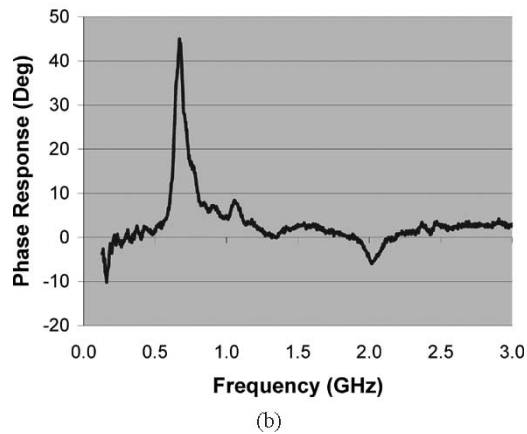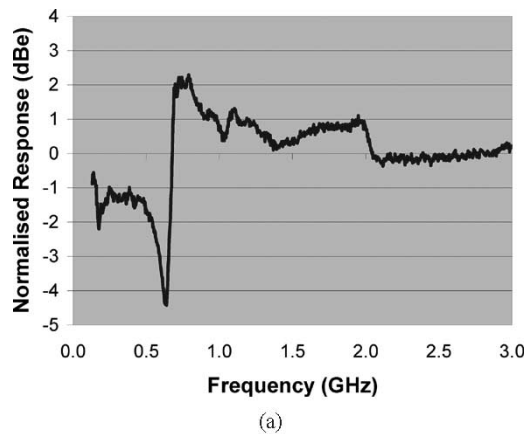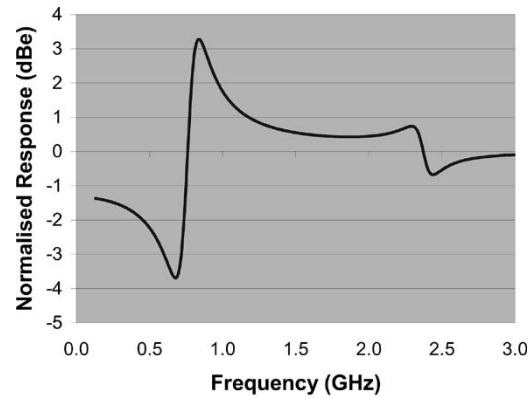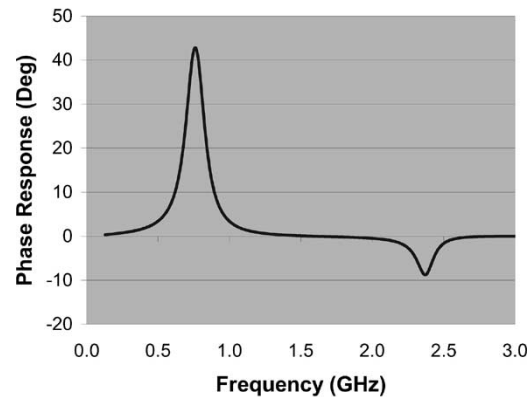

(a)

(b)

Fig. 5. Measured TE response (device K9m2d4, $g = 3.3$, $h = 3.5$). (a) Magnitude. (b) Phase.

(a)

(b)

Fig. 6. Theoretical TE response ($Z_1 = 4 \times 10^6$, $g = 3.3$). (a) Magnitude. (b) Phase.

TABLE I
MATERIAL PARAMETERS USED IN 1-D MODEL [1], [10]

Parameter	GaAs (core region)
Density (kg/m³)	
ρ	5360
Stiffness (N/m²)	
c_{11}	11.88×10^{10}
c_{12}	5.38×10^{10}
c_{44}	5.94×10^{10}
Elastooptic Constants	
p_{11}	-0.165
p_{12}	-0.140
p_{44}	-0.072
Piezoelectic constant (C/m²)	
e_{14}	-0.154
Electrooptic (m/V)	
r_{41}	-1.5×10^{-12}
Dielectric	
ε/ ε₀	12.85

and height of 3.3 and 3.5 μm, respectively. The SEM also shows that the modulator sidewalls are coated with 0.4 μm of a silicon nitride passivation layer. In this example, the depletion stop and the bottom of the waveguide core are 2.5 μm from the top of the ridge and so both are exposed by the deep etch.

Though the data in Fig. 4 show a regular behavior from 1–20 GHz, the data also show a significant deviation from flatness below 1 GHz. In Fig. 5, this low-frequency region is expanded and shows a severe anomaly in the response at approximately 700 MHz. This experimental data can be compared with the theoretical response that is displayed in Fig. 6. The theoretical response was computed from (13) and

used the material data in Table I [1], [10]. In these calculations, the acoustic impedance of the damping region Z_1 was selected to match the peak-to-peak variation of the theoretical results with that of experiment. It is seen that the theoretical response
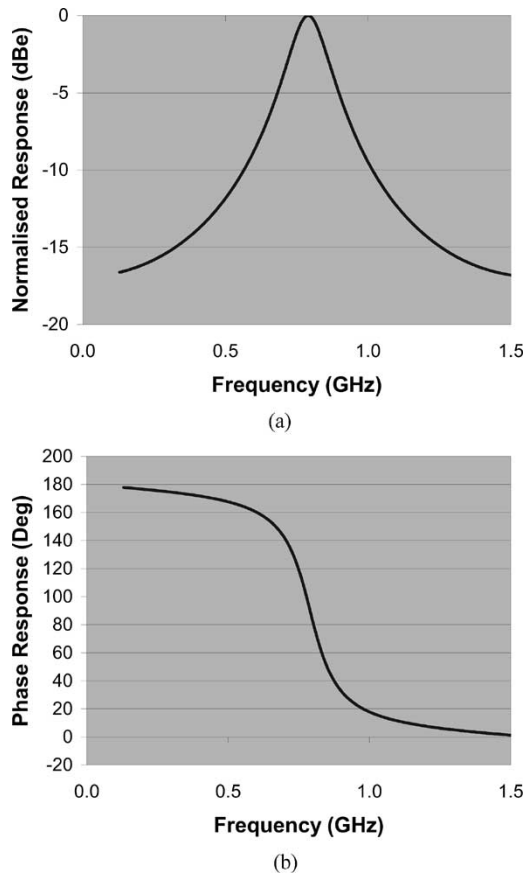
Fig. 7. Theoretical strain at center of waveguide core ($Z_1 = 4 \times 10^6$, $g = 3.3$). (a) Magnitude. (b) Phase.

Fig. 8. Measured TM response (device Q1c11, $g = 3.3$, $h = 5.1$). (a) Magnitude. (b) Phase.

displays many of the features that are evident in the measured data. These features are discussed in more detail hereafter.

A. Resonance Shape

The most obvious feature of the experimental data is the 700-MHz resonance. The shape of this resonance can be understood as follows: (10) shows that the maximum strain in the waveguide core is at $x = 0$. Because the spatial form of $S_{xx}^c(x)$ and, hence, the averaging implied by (13) does not change significantly across the resonance, the frequency response of the elastooptic effect can be inferred from $S_{xx}^c(0)$. In Fig. 7, the magnitude and phase of $S_{xx}^c(0)$ is plotted as a function of frequency in the region of the anomaly and shows that the mechanical vibration has the form of a forced, damped oscillator. Below the resonant frequency, this mechanical oscillation is in phase with the applied field that is forcing the mechanical vibration, and as a consequence, the modulator response is reduced because the elastooptic effect opposes the electrooptic effect. This cancellation becomes more pronounced as the drive frequency approaches resonance because of the increasing amplitude of the mechanical oscillation. As the frequency passes through the resonance, the phase of the mechanical oscillation changes, relative to driving field, by close to $180°$. Therefore, above the resonance, the elastooptic effect adds to the electrooptic effect and leads to peak in the modulator response. The half-width and magnitude of the peak will depend upon the Q of the mechanical oscillation, and in the 1-D model, this is determined by the leakage of acoustic
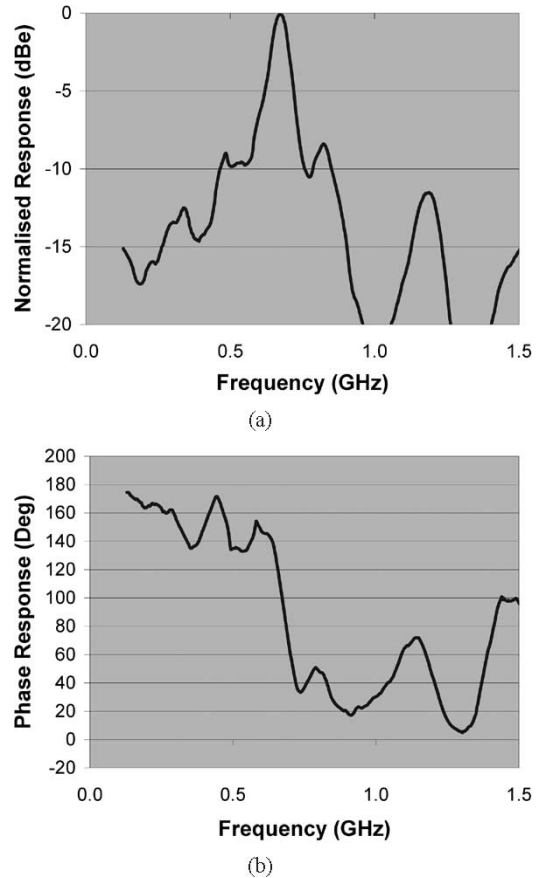
energy into the damping regions. In a real device, the Q is limited by a number of factors, including material damping and coupling to both bulk and surface acoustic waves.

Direct evidence of the elastooptic effect and the behavior of $S_{xx}^c(0)$ about the resonant frequency can be inferred from the TM response of the modulator. The TM response is displayed in Fig. 8 and was measured using the HP8703a with the polarizers set to pass TM-polarized light. While the data in Fig. 8(a) are consistent with the resonant behavior that is seen in Fig. 7(a), the phase response, shown in Fig. 8(b), is more difficult to interpret. Unfortunately, because the modulators used in this study were not designed to transmit TM-polarized light, the optical loss was high for this polarization leading to noise in our measurements. However, if attention is restricted to frequencies that are ± 50 MHz about the resonance, where the TM response is strongest, then the response shows an abrupt change in phase that is consistent with Fig. 8(b).

B. Resonant Frequencies

The frequencies at which the ridge can undergo mechanical resonance f_r are given by

$$f_r = \frac{m v_p^{\text{GaAs}}}{2w} \tag{14}$$

where m is an odd integer and v_p^{GaAs} is the longitudinal acoustic wave velocity in GaAs along the $[0\bar{1}1]$ direction. The even modes of vibration are excluded from (14) by the requirement that the center of the ridge is a displacement node.

Consequently, only the first- and third-order vibrations are seen in Fig. 5. The experimental data also suggest that the size of the resonances decrease with increasing order. This behavior is attributed to the spatial averaging implied by (13) and also to an increased acoustic loss at higher frequencies.

A careful examination of the experimental data also shows that the theory overestimates the resonant frequencies by approximately 10%. Much better agreement is obtained, however, when the passivation on the ridge sidewalls is included as this layer increases the effective width of the ridge.

C. Step in the Optical Response

Fig. 5 shows that there is a step in the optical response between 130 MHz and 3 GHz. This type of behavior is seen in other EOMs and is caused by the change in the electrooptic coefficients between the unclamped and clamped states [11], [12]. The relationship between clamped and unclamped electrooptic coefficients, the piezoelectric effect, and the elastooptic effect is readily understood with reference to the 1-D model: when a static electric field is applied to the waveguide core in Fig. 3, and no mechanical constraint is applied, the stress-free condition $T_{xx}(\pm a) = 0$, together with Fig. 6(a), implies that $S_{xx}(x)$ is a constant directly proportional to E_y. In this case, the elastooptic contribution to Δn^{TE} cannot be distinguished from the electrooptic component. Consequently, a composite electrooptic coefficient that includes both electrooptic and elastooptic contributions can be defined as

$$r_{41}^U = r_{41} + \frac{(p_{11} + p_{12} + 2p_{44})}{(c_{11} + c_{12} + 2c_{44})} e_{14}. \tag{15}$$

r_{41}^U is known as the unclamped electrooptic coefficient. At high frequencies where crystal inertia prevents a macroscopic strain, the crystal is said to be "clamped" and the electrooptic coefficient reverts to r_{41}. Substituting the data from Table I into (15) suggests that the modulator response will exhibit a step of 1.5 dB between dc and high frequencies. This is consistent with experimental observations.

IV. CONCLUSION

EOMs based on deep-etched waveguides with vertical sidewalls are susceptible to the generation and confinement of acoustic waves. At critical frequencies, a transverse acoustic resonance of the ridge can occur that results in elastooptic-induced anomalies in the modulator response. In this paper, the theory of acoustooptic interactions in linear EOMs was described, and a 1-D model of deep-etched GaAs–AlGaAs modulators was presented. This model was compared against experiment and good agreement was found.

ACKNOWLEDGMENT

REFERENCES

[1] R. G. Walker, "High speed III–V semiconductor intensity modulation," *IEEE J. Quantum Electron.*, vol. 27, pp. 654–667, Mar. 1991.

[2] R. G. Walker, R. Griffin, R. Harris, R. Johnstone, N. Perney, and N. Whitbread, "Integrated high functionality GaAs modulators for 10 & 40 Gb/s transmission," in *Integrated Photonics Research*, OSA Dig. ISBN 1-55 752-672-9, Monterey, CA, 2001, IME3-1.

[3] R. A. Griffin, R. I. Johnstone, R. G. Walker, J. Hall, S. D. Wadsworth, K. Berry, A. C. Carter, M. J. Wale, J. Hughes, P. A. Jerram, and N. J. Parsons, "10 Gb/s optical differential quadrature phase shift key (DQPSK) transmission using GaAs/ AlGaAs integration," presented at the Optical Fiber Communications Conf. (OFC'02), Anaheim, CA, 2002, FD 6-1.

[4] R. A. Griffin, R. I. Johnson, R. G. Walker, S. D. Wadsworth, A. C. Carter, and M. J. Wale, "Integrated DQPSK transmitter for dispersion-tolerant and dispersion- managed DWDM transmission," presented at the Optical Fiber Communications Conf. (OFC'03), 2003.

[5] J. M. Heaton, C. D. Watson, S. B. Jones, M. M. Bourke, C. M. Boyne, G. W. Smith, and D. R. Wight, "Sixteen channel (1 to 16 GHz) microwave spectrum analyzer device based on phased array GaAs/ AlGaAs electro-optic waveguide delay lines," presented at the Photonics West Optoelectronics Conf. '98, San Jose, CA, 1998, 3278-30.

[6] J. M. Heaton, M. M. Bourke, S. B. Jones, B. H. Smith, K. P. Hilton, G. W. Smith, J. C. H. Birbeck, G. Berry, S. V. Dewar, and D. R. Wight, "Optimization of deep-etched, single-mode GaAs/AlGaAs optical waveguides using controlled leakage into the substrate," *J. Lightwave Technol.*, vol. 17, pp. 267–281, Feb. 1999.

[7] J. E. Nye, *Physical Properties of Crystals.* Oxford: Clarendon Press, 1985.

[8] C. Thompson and B. L. Weiss, "Characteristics of surface acoustic wave propagation in III–V semiconductor quantum well structures," *J. Appl. Phys.*, vol. 78, pp. 5002–5007, Oct. 1995.

[9] FlexPDE™, Finite Element Software. PDE Solutions, Inc.. [Online]. Available: http://www.pdesolutions.com

[10] C. Thompson and B. L. Weiss, "Acoustooptic interactions in AlGaAs-GaAs planar multilayer waveguide structures," *IEEE J. Quant. Electron.*, vol. 33, pp. 1601–1607, Sept. 1997.

[11] W. K. Burns, M. M. Howerton, R. P. Moeller, R. Krahenbuhl, R. W. McElhanon, and A. S. Greenblatt, "Low drive voltage, broad-band LiNbO$_3$ modulators with and without etched ridges," *J. Lightwave Technol.*, vol. 17, pp. 2551–2555, Dec. 1999.

[12] R. L. Jungerman, C. Johnsen, D. J. McQuate, K. Salomaa, M. P. Zurakowski, R. C. Bray, G. Conrad, D. Cropper, and P. Hernday, "High-speed optical modulator for application in instrumentation," *J. Lightwave Technol.*, vol. 8, pp. 1363–1370, Sept. 1990.

Christopher D. Watson, photograph and biography not available at the time of publication.

Maxime Poirier, photograph and biography not available at the time of publication.

John M. Heaton (M'98) was born in Skipton, U.K., in 1960. He received the B.Sc. degree in physics from Bristol University, Bristol, U.K., in 1982 and the D.Phil. degree in engineering science from Oxford University, Oxford, U.K., in 1986, with a dissertation on time-dependent volume holography in photorefractive crystals.

In 1985, he joined the Royal Signals and Radar Establishment, which became the Defence Evaluation and Research Agency (DERA) and is now QinetiQ, where he worked on microwave photonic devices in III–V semiconductors. His research concentrated in particular on high-frequency electrooptic waveguide devices for broad-band microwave transmission, radio-frequency signal processing, and 10-Gb/s long-haul telecom transmitters. In 2003, he joined Filtronic Compound Semiconductors, County Durham, U.K., where he now works on III–V optoelectronic components.

Dr. Heaton is a Member of the Optical Society of America (OSA).

Meirion Lewis, photograph and biography not available at the time of publication.

Marcel Boudreau, photograph and biography not available at the time of publication.